• Intelligent Ophthalmology •

Vault predicting after implantable collamer lens implantation using random forest network based on different features in ultrasound biomicroscopy images

Bin Fang[1], Qiu-Jian Zhu[2], Hui Yang[1], Li-Cheng Fan[1]

[1]School of Mechanical and Electrical Engineering, Soochow University, Suzhou 215100, Jiangsu Province, China
[2]Lixiang Eye Hospital of Soochow University, Suzhou 215021 Jiangsu Province, China
Co-first authors: Bin Fang and Qiu-Jian Zhu
Correspondence to: Li-Cheng Fan. School of Mechanical and Electrical Engineering, Soochow University, Suzhou 215100 Jiangsu Province, China. flcthy@126.com
Received: 2023-02-03 Accepted: 2023-08-02

Abstract

● **AIM:** To analyze ultrasound biomicroscopy (UBM) images using random forest network to find new features to make predictions about vault after implantable collamer lens (ICL) implantation.

● **METHODS:** A total of 450 UBM images were collected from the Lixiang Eye Hospital to provide the patient's preoperative parameters as well as the vault of the ICL after implantation. The vault was set as the prediction target, and the input elements were mainly ciliary sulcus shape parameters, which included 6 angular parameters, 2 area parameters, and 2 parameters, distance between ciliary sulci, and anterior chamber height. A random forest regression model was applied to predict the vault, with the number of base estimators (n_estimators) of 2000, the maximum tree depth (max_depth) of 17, the number of tree features (max_features) of Auto, and the random state (random_state) of 40.0.

● **RESULTS:** Among the parameters selected in this study, the distance between ciliary sulci had a greater importance proportion, reaching 52% before parameter optimization is performed, and other features had less influence, with an importance proportion of about 5%. The importance of the distance between the ciliary sulci increased to 53% after parameter optimization, and the importance of angle 3 and area 1 increased to 5% and 8% respectively, while the importance of the other parameters remained unchanged, and the distance between the ciliary sulci was considered the most important feature. Other features, although they accounted for a relatively small proportion, also had an impact on the vault prediction. After parameter optimization, the best prediction results were obtained, with a predicted mean value of 763.688 μm and an actual mean value of 776.9304 μm. The R^2 was 0.4456 and the root mean square error was 201.5166.

● **CONCLUSION:** A study based on UBM images using random forest network can be performed for prediction of the vault after ICL implantation and can provide some reference for ICL size selection.

● **KEYWORDS:** random forest network; ultrasound biomicroscopy images; vault prediction; implantable collamer lens

DOI:10.18240/ijo.2023.10.01

Citation: Fang B, Zhu QJ, Yang H, Fan LC. Vault predicting after implantable collamer lens implantation using random forest network based on different features in ultrasound biomicroscopy images. *Int J Ophthalmol* 2023;16(10):1561-1567

INTRODUCTION

Uncorrected myopia is now the leading cause of visual impairment worldwide and imposes a significant economic burden on society[1]. The prevalence of myopia is increasing every year, and World Health Organization (WHO) predicts that by 2050 the number of myopic people worldwide may reach 4.758 billion, including 938 million people with high myopia[2]. Therefore, there is a growing demand for refractive surgery. Keratomileusis remains as a traditional refractive surgery, which corrects myopia by changing the curvature of the anterior surface of the cornea to change the refractive power of the eye. However, because the surgery requires cutting corneal tissue, it can cause problems such as corneal dilation, dry eye, increased higher-order aberrations (HOAs), and limited surgical correction[3-4]. Implantable collamer lens (ICL) is an intraocular refractive surgery that has been repeatedly shown to be effective and stable, and is the preferred surgical procedure for patients with abnormal corneal morphology and high myopia because it does not require

corneal cutting and does not introduce HoAs[5-6]. In recent years, ICL implantation has developed rapidly, with more than one million successful ICL implantations[7]. With such a large volume of procedures, safety issues are particularly important, and most post-ICL complications are related to the vault. The vault refers to the distance between the posterior surface of the intraocular lens (IOL) and the anterior surface of the natural lens, and is an important indicator of safety after ICL implantation. A low vault can lead to mechanical friction between the IOL and the natural lens and obstruction of atrial water circulation in front of the natural lens, which can lead to the development of anterior subcapsular clouding and cataract formation[8-9]. Conversely, if the vault is too high, it can close the anterior chamber angle leading to the development of angle-closure glaucoma, and it can increase friction between the posterior surface of the iris and the IOL leading to increased pigment spreading syndrome, iris atrophy, and inflammation[10-13].

ICLs are available in four sizes, 12.1, 12.6, 13.2 and 13.7 mm, and choosing the right ICL size is key to achieving the desired vault after surgery. Unfortunately, however, there is no method to accurately predict the vault, and the recommendation given by the ICL manufacturers is to base the choice of crystal size on the white-to-white diameter (WTW) and anterior chamber depth (ACD), which is also the recommendation given by the Food and Drug Administration (FDA). However, according to the results of the Meta-analysis, the percentage of ideal vault that can be achieved by this method is about 83.6%, which is not enough[14]. The parameters of angle-to-angle distance, anterior chamber width, and lens loss height have also been analyzed by anterior segment optical coherence tomography (OCT) to predict the vault and make ICL size selection, and the highest study was able to achieve an ideal vault rate of about 91.2%[15]. And this seems to have reached a bottleneck and still a large proportion of patients do not achieve the desired vault.

Artificial intelligence is already widely used in ophthalmology[16-17]. Some scholars have also applied artificial intelligence to the field of refractive surgery. Shen *et al*[18] at Fudan University used artificial intelligence to analyze a database of 18 types of anterior segment parameters from 3536 patients and found that the random forest model had the best prediction for the vault, and the predictiveness of their model was 82.8%. Kamiya *et al*[19] at Kitasato University also applied artificial intelligence to analyze the anterior segment OCT database of 1745 subjects and found that the random forest-based machine learning model had the highest prediction accuracy. However, the aforementioned study was only retrospective, and even so, the accuracy was still not very satisfactory. The reason may be that the IOL is fixed in the ciliary sulcus both in the posterior chamber and anterior segment OCT cannot detect the posterior chamber structure, so the machine learning model based on anterior segment OCT both in the anterior segment measurement device may have some limitations.

The ultrasound biomicroscope (UBM) is the only device that can detect the ciliary sulcus, the posterior chamber structure of the eye. And some ciliary body features can significantly contribute to abnormal postoperative vault after ICL implantation. Chen *et al*[20] found a significant correlation between anterior ciliary body and excessive postoperative vault. However, UBM features such as anterior ciliary body are only a qualitative description of the image and they are difficult to translate into specific variables for the vault prediction.

Therefore, in this study, the ciliary sulcus morphology was quantified into some new features by analyzing only UBM images by artificial intelligence to try to predict the vault after ICL implantation. In the expectation that artificial intelligence can be applied to clinical practice and improve some reference for ICL size selection.

SUBJECTS AND METHODS

Ethical Approval The study was approved by the Ethics Committee of Soochow University (NO.SLER2019092), and the study procedures all followed the principles of the Declaration of Helsinki. Informed consent was obtained from each participant after a detailed explanation of the procedures prior to treatment. The names of all patients were concealed in this study.

Basic Information This study was a cross-sectional study. A total of 329 patients with 450 eyes with a mean age of 26.60±6.12y (range 18-45y) who underwent ICL implantation with a lens size selection of 13.2 mm at the Lixiang Eye Hospital of Soochow University between January 1, 2020 and December 30, 2021 were selected for the study, including 126 males with 197 eyes and 203 females with 253 eyes.

Preoperative Examination All patients underwent a complete preoperative examination, including uncorrected distance visual acuity (UCVA), best correct visual acuity (BCVA), computerized automated optometry, comprehensive optometry, noncontact tonometry (Canon Full Auto Tonometer TX-F; Japan), slit lamp examination, and fundoscopy. Anterior segment parameters, including steepest meridian keratometry (K1), flattest meridian angle measurement (K2), ACD, corneal thickness (CT), and horizontal WTW, were obtained by using an integrated anterior segment analyzer (Pentacam HR, OCULUS; Germany). Axial length (AL) was measured using an optical biometer (IOL Master 700, Carl Zeiss Meditec AG, Germany). The anterior segment morphology was acquired using a UBM (Solvay, Tianjin, China) equipped with a 50 MHz high-frequency sensing ultrasound probe with a transverse and longitudinal resolution of 40 μm. In panoramic mode, the scanning range was as wide as 17 mm and the depth was up to

Figure 1 UBM image and its processing A: Original UBM diagram (green line indicates the shape marked by the doctor); B: Ciliary sulcus shape interception using Labelme; C: Six angles of selection. UBM: Ultrasound biomicroscopy.

10 mm. Physiological saline was introduced. The patient was instructed to look at the ceiling marker at 4 m. After the patient was relaxed, the image with the correct eye position and the largest ciliary sulcus diameter was included in the study. The same examination was performed by the same technician or physician. All procedures were performed by the same experienced surgeon following standard surgical procedures without any intraoperative or postoperative complications. At 1mo postoperatively, patient vault was measured using Pentacam's 15-Picture HD mode.

Data Processing The data contained a total of 450 UBM images, of which 292 were randomly selected to be divided into the training set and the remaining 158 were used for the validation set. The labeling of the ciliary sulcus shape was performed by a physician. In this study, labelme was used to perform a more concise and clearer labeling based on the shape labeled by the physician (green part in Figure 1A), and the labeled shape features are shown in Figure 1B. The aim is to transform the ciliary sulcus shape variable into an angle variable and an area variable. Manual annotation of the selected specific angles is performed using the Opencv module in deep learning. Six angles need to be labeled in one image, as shown in Figure 1C. The more controversial angles are Angle 2, Angle 3, Angle 5, and Angle 6, where the distance between Angle 2 and Angle 5 is the width of the ciliary sulcus, and Angle 3 and Angle 6 are the two lowest angles of the ciliary sulcus. If the difference between any of the angles marked by the two persons during the marking process is greater than 5°, then the marking of the angle will be repeated. After three rounds of angle annotation, the average value is taken to obtain a new dataset. After obtaining the angle parameters, the automatic annotation of the two areas in Figure 1B was performed using Image J software. There are other parameters of anterior chamber height and the distance between ciliary sulci that have been given in Figure 1A. A total of 10 features were involved in the prediction in this study, and the vault parameter was the parameter to be predicted.

Vault Prediction This study applies random forest model for regression prediction. The random forest algorithm is an ensemble packing method that operates by constructing multiple decision trees in the training phase. Most of the output (tree) decisions are selected by the random forest as the final decision. The main advantage of using random forests is that it mixes two supervised learning problems, namely regression and classification. "A random forest consists of a disproportionate number of independent decision trees that operate as an ensemble, where each tree in the random forest gives a category prediction, and then the category with the most votes become the prediction for this research model[21]." Measuring the relative importance of each feature to the prediction is another advantage of the random forest algorithm. Another advantage of the random forest algorithm is that it is also simple. In a random forest, each tree is selected from a random subset of features. This high level of variation leads to less correlation between trees and more diversity. A total of 10 features were used for the input of parameters. In this study, the ICL size was removed from the features this time, *i.e.*, the same type of crystal size was used for all of them. After screening and observation, the data sample size and the size of the lens selected for the real procedure were taken into account. A total of 450 UBM images with a 13.2 mm implant were selected for this study.

The random forest used in this study determined the importance of features by measuring their contribution to regression performance. The idea of the evaluation is Gini importance (or average reduction of impurities). For each feature, gather how evenly it reduces impurities. The average of all trees in a forest is a measure of the importance of a feature. This approach is available in the scikit-learn implementation of random forests (for classifiers and regressors). The variable importance measure is represented by VIM, and the Gini index is represented by GI. It is assumed that there are J features X1, X2,… Xj, I decision trees, C categories. Now it is necessary to calculate the Gini index score VIM of each feature Xj, that is, the average change of node splitting impurity of the JTH feature in all decision trees of random forest. The calculation formula of Gini index of the ith tree node q is[22]

$$GI_q^{(i)} = \sum_{c=1}^{|C|} \sum_{c' \neq c} P_{qc}^{(i)} P_{qc'}^{(i)} = 1 - \sum_{c=1}^{|C|} \left(P_{qc}^{(i)}\right)^2 \quad (1)$$

Where, C represents that there are C categories, and P_{qc} represents the proportion of category c in node q. The importance of feature Xj in the ith tree node q, that is, the Gini

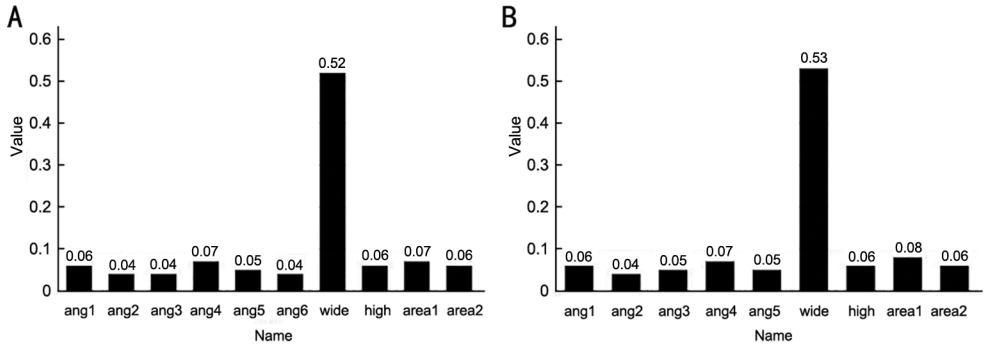

Figure 2 Percentage of importance of each feature after the participation of different features in the prediction A: Ten features are involved in prediction; B: Removal of Angle 6 feature.

index change before and after the branch of node q is

$$VIM_{jq}^{(Gini)(i)} = GI_q^{(i)} - GI_l^{(i)} - GI_r^{(i)} \quad (2)$$

Where, $GI_l^{(i)}$ and $GI_r^{(i)}$ respectively represent the Gini indices of the two new nodes after tree splitting. If the node where feature Xj appears in decision tree i is set Q, then the importance of Xj in the ith tree is

$$VIM_j^{(Gini)(i)} = \sum_{q \in Q} VIM_{jq}^{(Gini)(i)} \quad (3)$$

So let's say I trees in the random forest, so

$$VIM_j^{(Gini)(i)} = \sum_{i=1}^{I} VIM_j^{(Gini)(i)} \quad (4)$$

Finally, all the importance scores are normalized

$$VIM_j^{(Gini)(i)} = \frac{VIM_j^{(Gini)}}{\sum_{j'=1}^{J} VIM_{j'}^{(Gini)}} \quad (5)$$

After determining the optimal parameters, backward selection was performed based on the ranking of feature importance in the random forest model to find the best set of input features.

Statistical Analysis The analysis software was SPSS 22.0, and the measures were expressed in the form of mean±standard deviation. The R^2 score of goodness of fit and root mean square error (RMSE) were used as indicators for the assessment of regression models. Independent samples *t*-test was used to compare the clinical information in the training and validation sets. Predicted and actual vault were analyzed for agreement using the Bland-Altman test, and the absolute values of the differences between predicted and actual vault were calculated in the intervals of <100, 100 to 200, 200 to 300, 300 to 400, and 400 μm. P<0.05 was considered statistically significant difference.

RESULTS

Baseline Information The final 292 UBM images from 208 subjects with a mean age of 27.01±6.29y were categorized as the training set; 158 UBM images from another 121 subjects with a mean age of 25.84±5.73y were categorized as the validation set. The rest of the clinical data are detailed in Table 1.

Table 1 Baseline information of the two data sets mean±SD

Clinical parameter	Train	Test	*P*
Postoperative vault, μm	547.13±201.33	538.04±188.52	0.64
Age, y	27.01±6.29	25.84±5.73	0.05
IOP, mm Hg	13.03±2.37	13.47±2.72	0.07
WTW, mm	11.83±0.29	11.87±0.35	0.13
GTG, mm	11.83±0.29	11.86±0.32	0.21
ACD, mm	3.33±0.22	3.37±0.24	0.09
K1, D	42.41±1.21	42.25±1.38	0.19
K2, D	43.94±1.45	43.68±1.38	0.06
OA, mm	27.07±1.33	27.15±1.29	0.55
SE, D	-7.91±2.51	-8.02±2.35	0.66

IOP: Intraocular pressure; WTW: White to white; GTG: Groove to groove; ACD: Anterior chamber depth; K1: Steepest meridian keratometry; K2: Flattest meridian keratometry; OA: Anteroposterior axis; SE: Spherical equivalent.

Image Analysis After inputting all 10 features, the importance percentages are shown in Figure 2A. The importance share of the distance between the ciliary sulci is 52%, which is consistent with the doctor's conclusion. The other parameters accounted for a lower percentage, all around 5%. Subsequently, this study tried to input different parameters, and sorted and accumulated the features according to their importance ratio. When the cumulative importance of features reached 95%, the accumulated features were selected for re-prediction, while other features were abandoned. As shown in Figure 3, the feature to be discarded is Angle 6. After the removal of Angle 6, the distance between ciliary sulci increased to 53%, and the importance shares of other features were shown in Figure 2B, where the importance shares of Angle 3 and Area 1 increased to 5% and 8%. The mean predicted value was 763.688 μm and the mean actual value was 776.9304 μm, and the mean error between predicted and actual was -13.2424 μm. The statistical results of the absolute value of the error between predicted and true values and their percentages are shown in Figure 4. The number of differences less than or equal to 100 μm is 65, accounting for 41%, the number of differences between 100 and 200 μm is 42, accounting for 27%, the number of

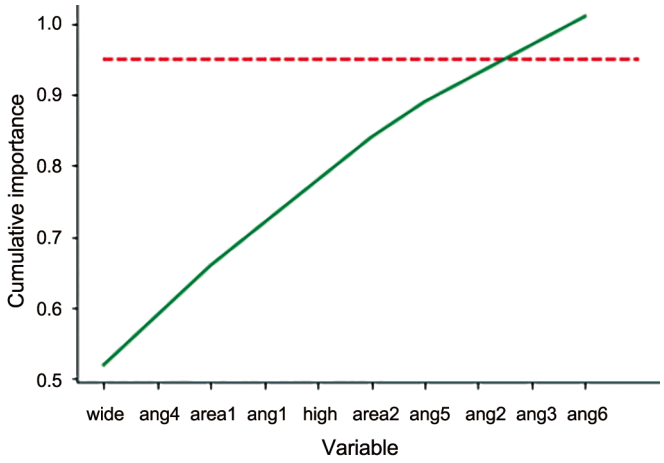

Figure 3 Cumulative plot of feature importance.

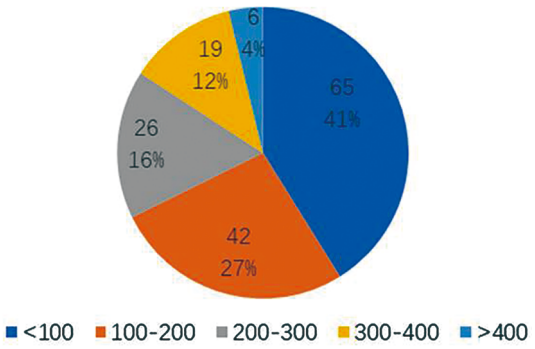

Figure 4 The number of differences between predicted and true values and their percentages.

differences between 200 and 300 μm is 26, accounting for 16%, the number of differences between 300 and 400 μm is 19, accounting for 12, and the number of differences greater than 400 μm is 6, accounting for 12. The number of the differences between 300 and 400 μm was 19, accounting for 12, and the number of differences greater than 400 μm was 6, accounting for 4%. The absolute value of the prediction error within 300 μm is 84%.

Bland-Altman analysis (Figure 5) showed that the average difference between the predicted vault of ICL and the predicted actual vault obtained using random forest (95% confidence interval) was -13.24±201.1 μm (-407.4 to 380.9 μm). The R^2 increased from 0.4366 to 0.4456 and the RMSE decreased from 203.1328 to 201.5166 after Angle 6 removal, and the changes of R^2 and RMSE before and after Angle 6 removal are shown in Table 2.

DISCUSSION

The demand for refractive surgery is booming worldwide. ICL implantation has shown outstanding efficacy in refractive error correction[23-25], with promising applications. However, the safety of the procedure is closely related to the appropriate ICL size and the high ICL arch after implantation.

In this study, 10 feature parameters were screened, trained and tested with a random forest model to predict the vault after

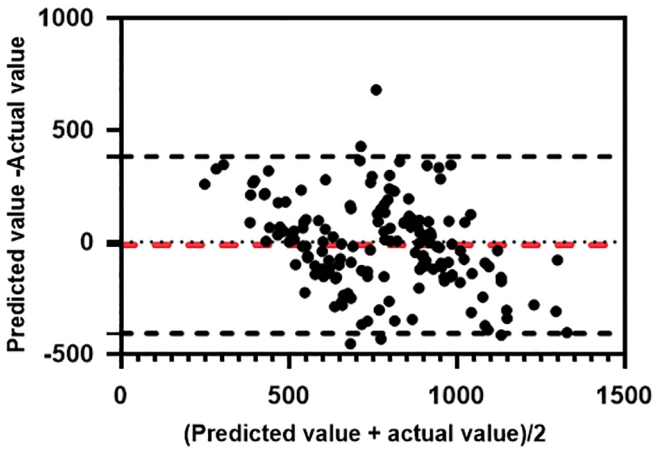

Figure 5 Consistency analysis diagram.

Table 2 R^2 and RMSE before and after Angle 6 removal

Features	R^2	RMSE
All features	0.4366	203.1328
Removal of Angle 6 features	0.4456	201.5166

RMSE: Root-mean-square error.

ICL implantation. In this study, UBM images of patients with 13.2 mm lens implantation were selected for the study, so the parameter ICL size no longer influenced the results, although the article showed that ICL size has a large effect on the vault of the implanted lens[26], but the main purpose of this study was to find other valuable parameters for vault prediction in UBM images. Among all parameters, the width between the ciliary sulci was the most important one, which is consistent with the findings of previous studies. Meanwhile, the other angular as well as area parameters accounted for a small percentage of importance, but they would have some influence on the prediction results. It indicates that the above angular and area parameters should not be ignored when predicting the vault or guiding ICL size.

In this study, parameters were added or subtracted for some parameters that accounted for less importance to observe the effect of the model. In the random forest model, the parameters were kept constant and only Angle 5, Angle 2, Angle 3, and Angle 6 were reduced. This indicates that some features can confound the prediction, and the more features are selected, the better the prediction results will be.

The vault is a key parameter for postoperative safety, and in this study, we conducted a study of new features in UBM images for implantation of ICL vault using a random forest model to evaluate the effect of different feature parameters on prediction, and the fit R^2 value reached 0.44. Comparing with the R^2 of 0.315 obtained in Shen *et al*[18], the R^2 in this study has a large increase, but the RMSE has increased. One possible explanation is that the eye size parameter is a continuously normally distributed variable. In contrast, ICL sizes are noncontinuous (only four sizes available) and one ICL size

was chosen for this trial, which could not fit all patients, resulting in large deviations in vault in the population after ICL implantation. In addition, the vault can change over time. The exact value of the vault value may not be determined. In practice, it is not necessary to predict the exact value of the vault. Reliable predictions of the likely range of vaults may be more appropriate to guide ICL sizing so that a safe vault height can be achieved after operation.

There are some limitations in this study. Because this study is a cross-sectional study and not a longitudinal study, changes in the vault over time were not assessed and remain unknown. Long-term follow-up is critical for predicting changes in the vault over time; only UBM images of patients with a single crystal size were used in this study and the sample data size was small, which leads to some values that can adversely affect the prediction. More sample data are needed to be added to the predictions at a later stage. In addition, the feature selection and labeling were performed in a more subjective way, especially for the angular parameters. Subsequent automatic identification as well as labeling can reduce the impact of subjective errors with less workload. In addition, this study mainly involves ciliary sulcus features, and the prediction may be more accurate if some previous features such as WTW are added.

In the future study, it is necessary to go more deeply to solve some errors in the dataset in the initial as well as subsequent annotation, which can reduce some errors due to larger errors; explore more features for prediction, and will try to introduce some external data through collaboration and combine different modality data (such as UBM or anterior segment OCT data), hoping to predict more accurately the postoperative vault; a single size was selected for vault prediction in this study, and subsequent vault predictions for four different crystal sizes will be required, which will require a much larger data set. And with fewer patients implanted with 12.1 or 13.7 mm crystals, direct prediction will result in not good results, which is a concern for the follow-up study.

In conclusion, artificial intelligence is of great help to the diagnosis and screening of eye diseases[27-29], which is applicable to vault prediction and ICL size determination. In this paper, we tried to find new features for predicting the vault of implanted ICL crystalline lenses. The results show that our newly selected ciliary sulcus feature can be more effective in predicting the vault for the purpose of giving a reference for ICL size selection.

ACKNOWLEDGEMENTS

Conflicts of Interest: Fang B, None; **Zhu QJ,** None; **Yang H,** None; **Fan LC,** None.

REFERENCES

1 Naidoo KS, Fricke TR, Frick KD, Jong M, Naduvilath TJ, Resnikoff S, Sankaridurg P. Potential lost productivity resulting from the global burden of myopia: systematic review, meta-analysis, and modeling. *Ophthalmology* 2019;126(3):338-346.

2 Sankaridurg P, Tahhan N, Kandel H, Naduvilath T, Zou HD, Frick KD, Marmamula S, Friedman DS, Lamoureux E, Keeffe J, Walline JJ, Fricke TR, Kovai V, Resnikoff S. IMI impact of myopia. *Invest Ophthalmol Vis Sci* 2021;62(5):2.

3 Murueta-Goyena A, Cañadas P. Visual outcomes and management after corneal refractive surgery: a review. *J Optom* 2018;11(2):121-129.

4 Alfonso-Bartolozzi B, Martínez-Alberquilla I, Baamonde B, Fernández-Vega-Cueto L, Alfonso JF, Madrid-Costa D. Refractive surgery after deep anterior lamellar keratoplasty: a review of the literature. *Int Ophthalmol* 2023;43(4):1413-1435.

5 Niu LL, Miao HM, Tian M, Fu D, Wang XY, Zhou XT. One-year visual outcomes and optical quality of femtosecond laser small incision lenticule extraction and Visian Implantable Collamer Lens (ICL V4c) implantation for high myopia. *Acta Ophthalmol* 2020;98(6):e662-e667.

6 Montés-Micó R, Ruiz-Mesa R, Rodríguez-Prats JL, Tañá-Rivero P. Posterior-chamber phakic implantable collamer lenses with a central port: a review. *Acta Ophthalmol* 2021;99(3):e288-e301.

7 Kim T, Kim SJ, Lee BY, Cho HJ, Sa BG, Ryu IH, Kim JK, Lee IS, Han E, Kim H, Yoo TK. Development of an implantable collamer lens sizing model: a retrospective study using ANTERION swept-source optical coherence tomography and a literature review. *BMC Ophthalmol* 2023;23(1):59.

8 Gimbel HV, LeClair BM, Jabo B, Marzouk H. Incidence of implantable Collamer lens-induced cataract. *Can J Ophthalmol* 2018;53(5):518-522.

9 Choi JH, Lim DH, Nam SW, Yang CM, Chung ES, Chung TY. Ten-year clinical outcomes after implantation of a posterior chamber phakic intraocular lens for myopia. *J Cataract Refract Surg* 2019;45(11):1555-1561.

10 Chun YS, Park IK, Lee HI, Lee JH, Kim JC. Iris and trabecular meshwork pigment changes after posterior chamber phakic intraocular lens implantation. *J Cataract Refract Surg* 2006;32(9):1452-1458.

11 Ye C, Patel CK, Momont AC, Liu Y. Advanced pigment dispersion glaucoma secondary to phakic intraocular collamer lens implant. *Am J Ophthalmol Case Rep* 2018;10:65-67.

12 Shipper I. Surgical management of acute angle-closure glaucoma after implantation of a toric ICL. *J Cataract Refract Surg* 2007;33(4):563-564.

13 Mastromonaco C, Balazsi M, Saheb N, Salimi A, Burnier MN Jr. Histopathological changes in the anterior segment with anterior and posterior chamber intraocular lens. *Can J Ophthalmol* 2020;55(5):437-444.

14 Packer M. Meta-analysis and review: effectiveness, safety, and central port design of the intraocular collamer lens. *Clin Ophthalmol* 2016;10:1059-1077.

15 Nakamura T, Isogai N, Kojima T, Yoshida Y, Sugiyama Y. Optimization of implantable collamer lens sizing based on swept-

source anterior segment optical coherence tomography. *J Cataract Refract Surg* 2020;46(5):742-748.

16 Cao YT, Che DY, Pan YL, *et al*. Artificial intelligence improves accuracy, efficiency, and reliability of a handheld infrared eccentric autorefractor for adult refractometry. *Int J Ophthalmol* 2022;15(4): 628-634.

17 Du XL, Li WB, Hu BJ. Application of artificial intelligence in ophthalmology. *Int J Ophthalmol* 2018;11(9):1555-1561.

18 Shen Y, Wang L, Jian WJ, Shang JM, Wang X, Ju L, Li MY, Zhao J, Chen X, Ge ZY, Wang XY, Zhou XT. Big-data and artificial-intelligence-assisted vault prediction and EVO-ICL size selection for myopia correction. *Br J Ophthalmol* 2023;107(2):201-206.

19 Kamiya K, Ryu IH, Yoo TK, *et al*. Prediction of phakic intraocular lens vault using machine learning of anterior segment optical coherence tomography metrics. *Am J Ophthalmol* 2021;226:90-99.

20 Chen Q, Tan WN, Lei XH, *et al*. Clinical prediction of excessive vault after implantable collamer lens implantation using ciliary body morphology. *J Refract Surg* 2020;36(6):380-387.

21 Tony Y. Understanding random forest: how the algorithm works and why it is so effective. Medium 2019. https://towardsdatascience.com/understanding-random-forest-58381e0602d2; Accessed on: Feb. 1st, 2023.

22 Nicodemus KK, Malley JD, Strobl C, Ziegler A. The behaviour of random forest permutation-based variable importance measures under predictor correlation. *BMC Bioinformatics* 2010;11:110.

23 Wang XJ, Chen D, Jiang Y, Chou YY, Luo Y, Li Y, Ma J, Zhong Y. The 100 most influential articles in myopia: a bibliometric analysis. *Int J Ophthalmol* 2022;15(1):150-156.

24 Wei RY, Li MY, Niu LL, *et al*. Comparison of visual outcomes after non-toric and toric implantable collamer lens V4c for myopia and astigmatism. *Acta Ophthalmol* 2021;99(5):511-518.

25 Feldhaus L, Mayer WJ, Dirisamer M, *et al*. Comparison of visual and refractive outcome between two methods of corneal marking for toric implantable collamer lenses (TICL) in phakic eyes. *Curr Eye Res* 2023;48(4):357-364.

26 Igarashi A, Shimizu K, Kato S, Kamiya K. Predictability of the vault after posterior chamber phakic intraocular lens implantation using anterior segment optical coherence tomography. *J Cataract Refract Surg* 2019;45(8):1099-1104.

27 Cao K, Xu J, Zhao WQ. Artificial intelligence on diabetic retinopathy diagnosis: an automatic classification method based on grey level co-occurrence matrix and naive Bayesian model. *Int J Ophthalmol* 2019;12(7):1158-1162.

28 Chen Q, Yu WH, Lin S, Liu BS, Wang Y, Wei QJ, He XX, Ding F, Yang G, Chen YX, Li XR, Hu BJ. Artificial intelligence can assist with diagnosing retinal vein occlusion. *Int J Ophthalmol* 2021; 14(12):1895-1902.

29 Ruan S, Liu Y, Hu WT, *et al*. A new handheld fundus camera combined with visual artificial intelligence facilitates diabetic retinopathy screening. *Int J Ophthalmol* 2022;15(4):620-627.